# In-situ green synthesis and adsorption on methylene blue of copper-based metal organic framework/cellulose/chitosan (CCTSA/HKUST-1) composite aerogel

TIANHAO WANG, LUYANG WANG, SHUN LIU, LIN CHEN, XIN JIN, HAITANG LIU, AND XIAOYUAN LIAO

**ABSTRACT:** In order to explore the application of metal-organic frameworks (MOFs) in environmental and water treatment fields, a new composite aerogel of HKUST-1/cellulose/chitosan (CCTSA/HKUST-1) with better hydrostability was synthesized by an in-situ synthesis method combining covalent cross-linking and solvothermal methods as an efficient adsorbent for methylene blue (MB). The composite aerogel (CCTSA) obtained by covalent cross-linking of cellulose (CE) and chitosan (CTS) exhibited excellent stability under strong acid and solvent-thermal conditions. With the increase of CTS content, it was beneficial to the in-situ synthesis of HKUST-1, as well as to increase the mass loading rate of HKUST-1 to 37.06%, while the Brunauer-Emmett-Teller (BET) specific surface area of CCTSA/HKUST-1 composite aerogel reached 945.123 $m^2 \cdot g^{-1}$, which was much higher than that of the CCTSA composite aerogel (14.489 $m^2 \cdot g^{-1}$). The CCTSA/ HKUST-1 composite aerogel exhibited excellent adsorption capacity (537.6 $mg \cdot g^{-1}$) on MB solution, and cyclic adsorption could be achieved.

This study proposes a concept of valorization of alkaline peroxide mechanical pulping (APMP) waste liquor to hemicellulose-based hydrogel. This hemicellulose-based hydrogel exhibits a sensitive temperature/pH dual response. Hemicellulose-based hydrogels swell or shrink through the change of hydrogen bond/electrostatic repulsion/charge screening. They also show good water absorption and water retention properties.

***Application:*** This study can give ideas for the preparation of stable, high specific surface area and high adsorption capacity polysaccharide-based aerogel adsorption materials and enrich the application of MOFs materials in the field of water treatment and organic dye adsorption.

The rapid population growth and increased industrialization of the last few decades have been accompanied by increasingly serious environmental pollution problems; for example, soil, water and air pollution, with water pollution being a particularly serious problem [1-3]. Studies have shown that most countries will face a serious water crisis in the next few decades or so [2]. As the most common organic pollutant, dyes mainly originate from textile and dyeing plants, paper factories, and domestic wastewater discharges, with about 100 metric tons of contaminated water with dyes being discharged into the wastewater each year [4]. Methylene blue (MB), an organic cationic dye, is a typical azo dye that is not easily biodegradable due to the molecular structure of the benzene ring, which not only deteriorates water quality, but is mutagenic, genotoxic, and carcinogenic, and can have a number of harmful effects on humans [4,5].

At present, the commonly used wastewater treatment methods include coagulation, adsorption, membrane separation, photocatalysis, and so on [6]. The advantages of easy operation, mild conditions, low cost, and the possibility of cyclic adsorption have made it a commonly used method in the field of wastewater treatment [7]. Normal adsorbents include natural clay, activated carbon, zeolite, and so on. However, due to their low adsorption capacity, high cost, and non-biodegradability, adsorbents are very limited in practical application [8]. In recent years, natural polysaccharides have gained popularity in wastewater treatment due to their wide source of raw materials, low cost, good biocompatibility, and biodegradability [9,10].

Cellulose (CE) is the most abundant linear polysaccharide in nature and is characterized by its high strength and excellent water stability, and the use of cotton fiber is more economical and environmentally friendly than the use of nanocellulose (cellulose nanofibrils; CNF) in the preparation of regenerated cellulose composite aerogels [11-13]. Chitosan (CTS) is the second most abundant polysaccharide in nature and rich in amine and hydroxyl groups, which makes it an ideal adsorbent for wastewater treatment [14,15]. Both are also excellent substrates for the preparation of various 3D hydrogels or aerogels. Some studies have reported that although the mechanical strength of the composite aerogel prepared by simple blending of the two is improved to a certain extent, this

highly porous structure is unstable in an aqueous environment for a long time due to the absence of covalent cross-linking reactions [16].

The use of advanced porous materials to remove organic pollutants from water shows promise as a means of sustainable environmental remediation compared to polysaccharide aerogels [17-19]. Metal-organic frameworks (MOFs) are emerging porous materials with high porosity, high specific surface area, accessible adsorption sites, and adjustable pore size, formed by the interconnection of metal ion centers and organic ligands through self-assembly to form a class of porous materials with a three-dimensional periodic mesh skeleton. There are four main categories of MOFs: isoreticular metal-organic frameworks (IRMOFs), zeolitic imidazolate frameworks (ZIFs), materials of Institute Lavoisier frameworks (MILs), and pocket-channel frameworks (PCNs) [20-22]. A framework known as HKUST-1, as a representative of PCNs, has a high specific surface area, high porosity, and excellent water stability, making it an ideal adsorbent for wastewater treatment [4]. However, MOFs are usually found in powder form due to their poor alkali resistance and mechanical strength, and are somewhat brittle. To overcome these disadvantages, it is often necessary to give MOFs specific substrates (metal oxides, silica, polymers, graphene, carbon nanotubes, etc.) for actual use [23]. The preparation of MOFs composite aerogels by compounding MOFs with polymeric materials has proven to be an effective route, including MOFs/polysaccharide aerogels [24,25]. However, many MOFs are synthesized in processes with strong acids and high temperatures, and normal polysaccharide aerogels are prone to collapse and damage or low loading rates during such synthesis [26].

In this work, it was proposed to prepare an excellent stable aerogel (CCTSA) by covalently cross-linking CE and CTS, and then grow HKUST-1 in-situ under strong acid and solvent-thermal conditions to obtain an excellent stable CCTSA/HKUST-1 composite aerogel with high specific surface area and high adsorption capacity, and obtain an efficient MB adsorbent. The chemical composition, structure, and morphology of CCTSA/HKUST-1 aerogel were systematically characterized, as well as its adsorption capacity and mechanism on MB. The CCTSA/HKUST-1 showed a good adsorption capacity for MB and was able to achieve cyclic adsorption. This study will provide theoretical and technical support for the design and preparation of stable polysaccharide aerogel adsorbent materials with high adsorption capacity.

## EXPERIMENTAL

### Materials

The cotton pulp, with degree of polymerization of 800, was provided by Guangdong Zhongshun Paper Industry Group Co. Ltd. (Guangdong, China). The CTS (deacetylation degree ≥ 95%, viscosity 100-200 mpa.s) was purchased from Aladdin (Riverside, CA, USA). The N,N'-methylenebisacrylamide (MBA); trimesic acid (BTC, 98%); copper nitrate trihydrate ($Cu(NO_3)_2{\cdot}3H_2O$, 99%); potassium hydroxide (KOH, 95%); lithium hydroxide, anhydrous (LiOH, 98%); urea (99%); and MB were purchased from Macklin (Shanghai). All other solvents were used without further purification.

### Preparation of CCTSA/HKUST-1

Preparation of CCTSA

The cotton pulp (CE) was pretreated with a cutting grinder (SM300, Retsch; Haan, Germany) and dissolved in an aqueous solution of 4.6 wt% LiOH/15 wt% urea pre-cooled to -13.5°C. The 3 wt% CE solution was prepared by freezing and thawing three times [27]. The suspension was obtained by dispersing CTS powder in a pre-cooled (-30°C) 4.5 wt% LiOH, 7 wt% KOH, and 8 wt% urea aqueous solution under stirring, after which the suspension was frozen at -30°C for 4 h and completely thawed at room temperature (25°C). The 3 wt% CTS solution was prepared by freezing and thawing three times [28]. The two previously-described solutions with different mixing ratios (1:0.2,1:0.4,1:0.6, and 1:1) were mixed at low temperature (< 5°C) and stirred for 30 min with MBA at a molar ratio of 1:1 to the anhydroglucose units (AGU) of CE, and then centrifuged at 600 rpm for 5 min to obtain a homogeneous pre-gel solution. The mixed solution was poured into a polytetrafluoroethylene (PTFE) mold and kept at room temperature for 24 h to obtain CE/CTS hydrogel (CCTSH). The CCTSA aerogel was obtained by washing with deionized water to neutral and vacuum freeze-drying for 48 h.

Preparation of CCTSA/HKUST-1 by in-situ synthesis

The CCTSA aerogel (0.3 g) was infiltrated into 25 mL of 50% ethanol aqueous solution containing 5 mmol $Cu(NO_3)_2{\cdot}3H_2O$ and incubated (25°C) on a shaker of 80 rpm for 12 h. The BTC (3.5 mmol) was dissolved in 25 mL 50% ethanol aqueous solution and then added and stirred for 1 h. This was transferred to a PTFE hydrothermal reactor for 18 h (110°C). The aerogel matrix was removed from the solution and washed several times with 50% ethanol aqueous solution to remove the nonbonded HKUST-1 particles. The CCTSA/HKUST-1 aerogel was obtained after vacuum freeze-drying for 48 h [26].

### Calculation of HKUST-1 loading rate

The mass loading rate of HKUST-1 was calculated using thermogravimetric analysis data according to Eq. 1 [29]:

$$W_{HKUST-1} = \frac{m_{CCTSA/HKUST-1} - m_{CCTSA}}{m_{HKUST-1} - m_{CCTSA}} * \% \quad (1)$$

where $W_{HKUST-1}$ is the mass loading rate of HKUST-1; and $m_{CCTSA/HKUST-1}$, $m_{CCTSA}$, and $m_{HKUST-1}$ represent the residue contents of CCTSA/HKUST-1, CCTSA, and HKUST-1 at a given temperature, respectively.

### Characterization

The IR spectrum was tested on a VERTEX 70 FT/IR spectrophotometer (Bruker; Billerica, MA, USA) over the wavenumber range of 4000–500 $cm^{-1}$. The X-ray diffraction (XRD) spectra were measured at 5°–45° (4°/min) on an Empyrean diffractometer (Malvern Panalytical; Almelo, Netherlands). Thermogravimetric (TG) analyses of the samples were manipulated using a Hitachi 7200 analyzer (Tokyo, Japan) heated from room temperature to 800°C under nitrogen at the heating rate of 20°C·$min^{-1}$. The X-ray photoelectron spectroscopy (XPS) of ESCALAB 250Xi (Thermo Scientific; Waltham, MA, USA) was used to analyze the surface elements of MOFs composite aerogels and their chemical states. The test condition was Al-Kα (1486.6 eV). The nitrogen ($N_2$) sorption measurement was implemented on automatic volumetric adsorption equipment Autosorb-iQ (Quantachrome; Boynton Beach, FL, USA). All samples were analyzed after vacuum degassing at 105°C for 6 h. The specific surface area was calculated using the Brunauer-Emmett-Teller (BET) multilayer adsorption model, and the pore size distribution was calculated based on the quenched-solid-density-functional-theory (QSDFT) model. The microstructure and morphology of MOFs and composite aerogels were observed by scanning electron microscopy (JSM-IT300, JEOL; Tokyo). The isoelectric point of the composites was determined using the pH drift method (PHSJ-4A, Leici Electronic Co.; Shanghai, China).

### Adsorption experiments

A solution of MB in water at a concentration of 1000 mg·$L^{-1}$ was prepared and used to dilute it to the actual concentration required for the adsorption experiment. The absorbance of the MB solution before and after adsorption was measured by UV-Vis spectrophotometer at 664 nm. The pH value of the MB solution was adjusted with 0.01 M sodium hydroxide (NaOH) or 0.01 M hydrogen chloride (HCl) solution. The adsorption experiment was conducted by adding 0.03 g of adsorbent to 0.1 L of MB solution at room temperature. The CCTSA in the adsorption experiment refers to the composite aerogel formed by the molar ratio of the dehydrated glucose unit (AGU) of CE and the glucosaccharide unit (GSU) of CTS with a molar ratio of 1:1. The adsorption capacity ($q_t$) of the adsorbent on the MB solution was calculated according to Eq. 2 [4,30]:

$$q_t = \frac{V(c_0 - c_t)}{m} \tag{2}$$

where $V$ (L) is the volume of the MB solution; $c_0$ (mg·$L^{-1}$), and $c_t$ (mg·$L^{-1}$) correspond to the concentration of the MB solution initially and at time $t$ (h), respectively; $m$ (g) is the mass of the adsorbent; and the adsorption capacity at adsorption equilibrium is defined as the saturation adsorption capacity ($q_e$, mg·$L^{-1}$).

The adsorption kinetic model of CCTSA/HKUST-1 for MB solution is fitted by pseudo-first-order and pseudo-second-order kinetic models, as shown in Eq. 3 and Eq. 4 [4,30].

$$\log(q_e - q_t) = -\frac{k_1 t}{2.303} + \log q_e \tag{3}$$

$$\frac{t}{q_t} = \frac{1}{k_2 {q_e}^2} + \frac{t}{q_e} \tag{4}$$

where $q_e$ and $q_t$ are the adsorption capacities (mg·$g^{-1}$) when in equilibrium at time $t$ (h); and $k_1$($h^{-1}$) and $k_2$(g·$mg^{-1}$·$h^{-1}$) are the pseudo-first-order and pseudo-second-order rate constants, respectively.

The Langmuir and Freundlich adsorption isotherm models [4,30] are used to fit the adsorption isotherm model of CCTSA/HKUST-1 on MB solution, shown as follows:

$$\frac{c_e}{q_e} = \frac{1}{K_L q_{max}} + \frac{c_e}{q_{max}} \tag{5}$$

$$\log q_e = \log K_F + \frac{1}{n}\log c_e \tag{6}$$

where $K_L$ (L·$mg^{-1}$) and $q_{max}$ (mg·$g^{-1}$) are the Langmuir constants for the monolayer and adsorption energy related to $q_e$, respectively; and $K_F$ (mg·$g^{-1}$) and $n$ are the Freundlich constants representing the adsorption capacity and adsorption intensity, respectively.

The parameters ($\Delta H^o$, $\Delta S^o$, $\Delta G^o$) of adsorption thermodynamics are calculated by Eq. 7 and Eq. 8 based on the adsorption of CCTSA/HKUST-1 on MB solution at different temperatures [4,30].

$$\ln\frac{q_e}{c_e} = \frac{\Delta S^\circ}{R} - \frac{\Delta H^\circ}{RT} \tag{7}$$

$$\Delta G^\circ = \Delta S^\circ - T\Delta S^\circ \tag{8}$$

where $\Delta H^o$ and $\Delta S^o$ are the enthalpy change (KJ·$mol^{-1}$) and entropy change (J·$K^{-1}$·$mol^{-1}$) during adsorption, respectively; $\Delta G^o$ is the Gibbs free energy change (KJ·$mol^{-1}$); $R$ is the gas constant (8.314 J·$mol^{-1}$·$K^{-1}$); and $T$ is the absolute temperature (K).

### Regeneration experiments

Five adsorption-desorption cycle regeneration experiments were performed on CCTSA/HKUST-1 composite aerogels using MB solution at a concentration of 250 mg·$L^{-1}$ at pH 8.0. After the adsorption reached equilibrium, the adsorption capacity was determined as described above. The recovered composite aerogels were desorbed with anhydrous ethanol until the solution became colorless, washed with deionized water, and regenerated by freeze-drying. The reusability of the CCTSA/HKUST-1 composite aerogel was evaluated by the recovery efficiency (the percentage of

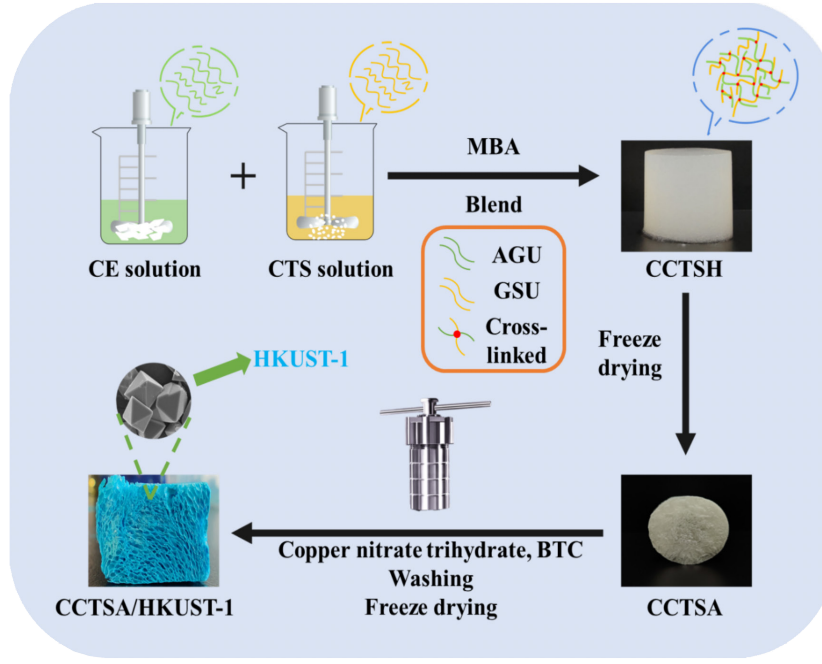


*1. Schematic diagram of the preparation steps of CCTSA/HKUST-1.*

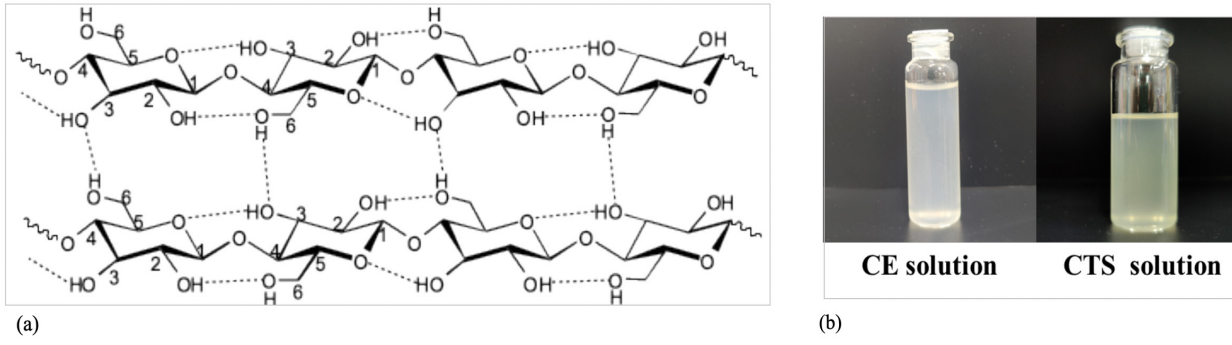


*2. (a) structure of cellulose (CE) diagram, and (b) dissolution of CE and chitosan (CTS).*

adsorption capacity of the regenerated composite aerogel to the adsorption capacity of the composite aerogel before regeneration).

## RESULTS AND DISCUSSION

### *Design of CCTSA/HKUST-1*

The process of synthesizing CCTSA/HKUST-1 is shown in **Fig. 1**. As shown in **Fig. 2a**, cellulose is a linear polymer linked by 1, 4-β-glycosidic bonds, with extremely strong intramolecular and intermolecular hydrogen bonding [31]. At low temperatures, the LiOH hydrate is more likely to combine with the hydroxyl groups on the cellulose to form a new hydrogen bonding network structure, thus breaking the original intramolecular and intermolecular hydrogen bonds of the cellulose and causing the cellulose to dissolve. Urea self-assembles in the outer layer of the cellulose and LiOH complex to form a channel inclusion compound, thus preventing cellulose molecules from aggregating [27,32]. Based on the similar structure of CE and CTS, the LiOH/urea system was used to freeze-thaw cycles at low temperature to obtain a uniform CE and CTS solution, as shown in Fig. 2b [28]. Then the crosslinker MBA was introduced and reacted with -OH groups in alkaline solution by Michael addition reactions to form ether bonds, in which intramolecular and intermolecular crosslinking may occur, as shown in **Fig. 3** [4,33]. Ultimately, CCTSA/HKUST-1 was obtained by in-situ synthesis. As shown in **Fig. 4**, HKUST-1 and the aerogel were mainly coordinated by copper ion ($Cu^{2+}$) and a large number of O and N atoms present in the aerogel, especially the introduction of N atoms, can complex the metal ions, thus improving the loading rate of MOFs, which can effectively prevent the possible risk of MOFs shedding [4,34].

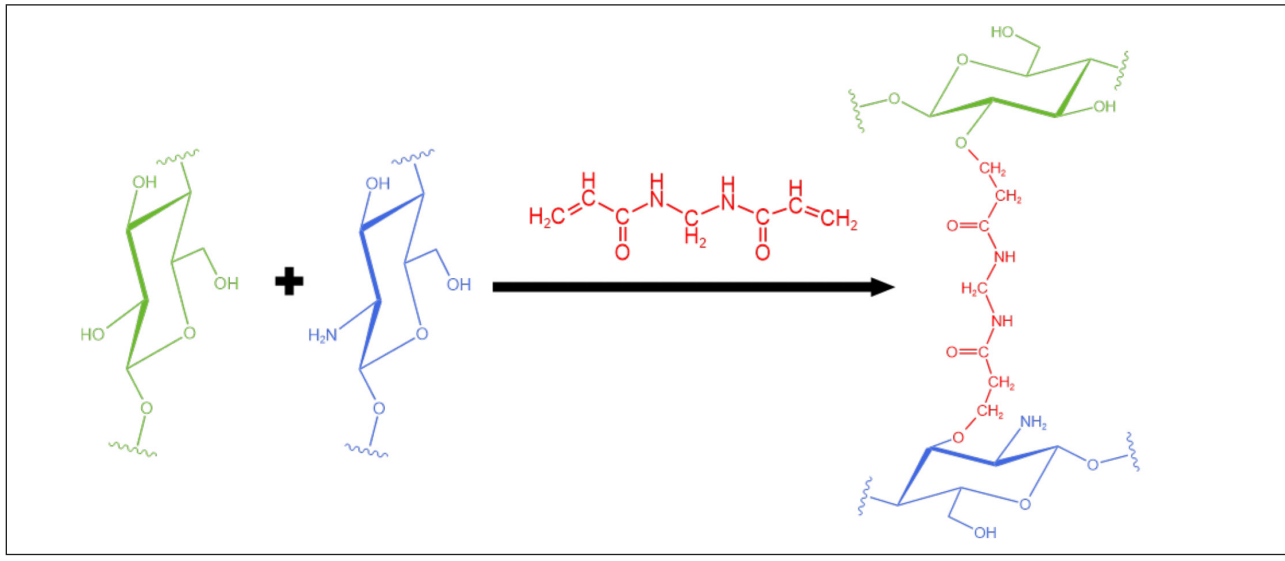

*3. The principle of covalent cross-linking.*

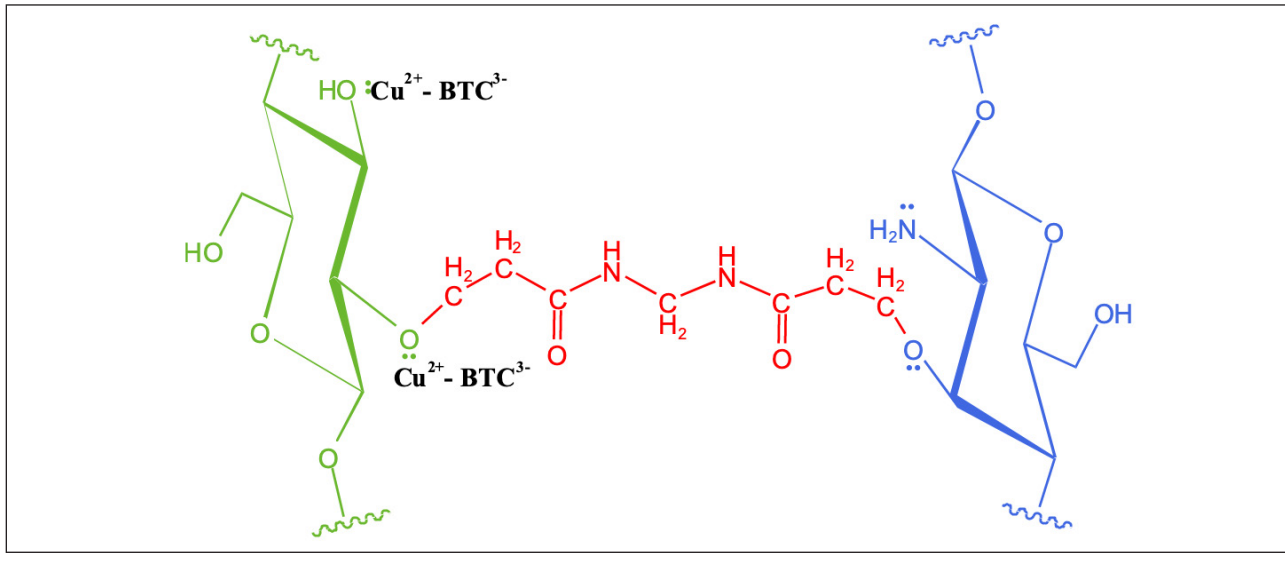


*4. The principle of in-situ synthesis of HKUST-1.*

### *Characterization of CCTSA/HKUST-1.*

The Fourier transform infrared (FTIR) spectroscopy analysis of CE is shown **Fig. 5**, with the characteristic peaks at 3428, 1633, 1428, 1372 and 1164 $cm^{-1}$ corresponding to the stretching vibration of -OH; the stretching vibration due to bound water; the absorption peak of $-CH_2$; the asymmetric stretching vibration of C-H; and the C-O-C vibration in the 1, 4-β glycosidic bond, respectively [35]. The characteristic peaks of CTS at 3414, 1615, 1322, 1080, 1028, and 896 $cm^{-1}$ correspond to the -OH and $-NH_2$ stretching vibration complex peaks; the N-H bending vibration; the C-N stretching vibration; the C-O stretching vibration on $C_3$; the C-O stretching vibration on $C_6$; and the β-configuration glycosidic bond characteristic peak, respectively [36,37]. The MBA represents -C=C-H and C=C stretching vibrations at 3063 and 1625 $cm^{-1}$, respectively, and -C=O stretching vibrations and -NH- bending vibrations are at 1657 and 1545 $cm^{-1}$, respectively. The CA is a cellulose aerogel made from CE solution with MBA, with peaks of -C=O stretching vibrations and -NH- bending vibrations (characteristic peaks of MBA) at 1657 and 1545 $cm^{-1}$, respectively, and the disappearance of the peaks at 3063 and 1625 $cm^{-1}$ represent the MBA double bond, indicating that the double bond was consumed in the reaction and the MBA was successfully grafted onto the cellulose chain [33,38]. The CCTSA is a composite aerogel produced with the addition of CTS. The -OH and $-NH_2$ form a broad absorption peak at 3448 $cm^{-1}$, and the C-N stretching vibration and the β-configuration glycosidic bonds represented at 1322 and 896 $cm^{-1}$, respectively, are intensified, which tentatively suggests that chemical cross-linking of cellulose and chitosan has occurred, resulting in the intensification of these two characteristic peaks [4,39]. The CCTSA/HKUST-1 is a composite aerogel loaded with HKUST-1. A peak representing the 1, 4-β gly-

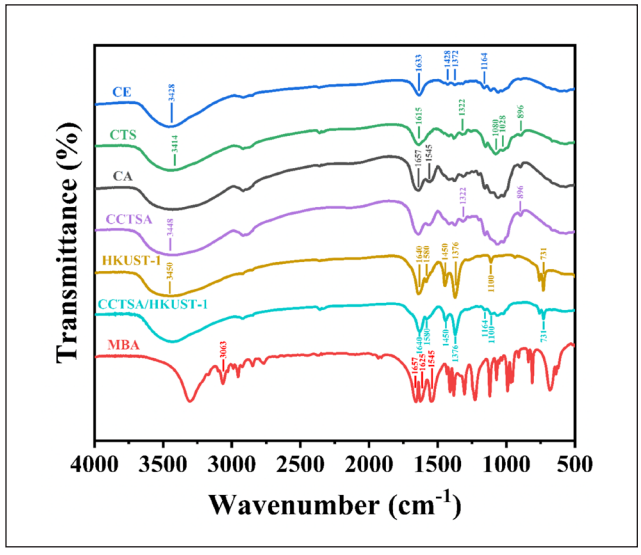


*5. Fourier transform infrared (FTIR) spectra of CCTSA/HKUST-1 composite aerogel and raw materials.*

cosidic bond of the polysaccharide at 1164 $cm^{-1}$ and a peak representing the Cu-O stretching vibration of HKUST-1 at 731 $cm^{-1}$ appear, indicating the successful loading of HKUST-1 on the composite aerogel [4,40].

As shown in **Fig. 6a**, the XRD comparison between the synthesized and simulated HKUST-1 shows that the XRD curves of the synthesized HKUST-1 in this work are in agreement with the simulated peak positions, indicating that HKUST-1 has been successfully synthesized [41]. The XRD comparison of CCTSA/HKUST-1 composite aerogels with different CTS contents ($CCTSA_{0.2}$/HKUST-1 represents the composite aerogel formed by $n_{AGU} : n_{GSU}=1 : 0.2$) is shown in Fig. 6b. It can be seen that the peak intensity corresponding to HKUST-1 in the CCTSA/HKUST-1 composite aerogel gradually increases with the increase of CTS content. This indicates that the CCTSA/HKUST-1 composite aerogel has been successfully produced and the presence of CTS is beneficial to the in-situ synthesis of HKUST-1, and the higher the content of CTS, the higher the loading rate of HKUST-1 [42,43].

An X-ray photoelectron spectroscopy (XPS) analysis is a powerful tool to further elucidate the interactions between HKUST-1 and CCTSA. As shown in **Fig. 7**, the XPS survey spectra of CCTSA and CCTSA/HKUST-1 includes the four elements Cu, C, O, and N. **Fig. 8a** and Fig. 8b correspond to the C1S high-resolution XPS spectra of CCTSA and CCTSA/HKUST-1, respectively. We can see that the main peaks of C-C, C-O, and C=O are located at typical positions 284.8 eV, 286.4 eV, and 288.4 eV, and the proportion of C=O and C-C increases significantly after loading HKUST-1, which may be attributed to successful in-situ synthesis of HKUST-1 and the introduction of -COO- groups, resulting in an increase in the ratio of C=O to C-C [26,29,44]. The O1s high-resolution XPS spectra of CCTSA/HKUST-1 is shown in Fig. 8c. The peaks of the signal at 533.1, 532.3, and 531.3 eV correspond to the C-OH, C-O, and C=O characteristic peaks of CCTSA/HKUST-1, respectively, indicating that the surface of CCTSA/HKUST-1 is covered with a large number of oxygen atoms [29,45]. The high-resolution XPS spectrum of Cu2p from CCTSA/HKUST-1 is shown in Fig. 8d. A "shake-up satellite band" indicating the paramagnetic chemical state of $Cu^{2+}$ appears between 940.5 and 944.3 eV. The characteristic peaks of Cu-O (934.9 eV) and Cu-N (932.8 eV) appear, with the binding energy of Cu-O being greater than that of Cu-N due to the electronegativity of the O atom that is greater than that of the N atom. It can also be seen that the relative intensity of the Cu-O peak is also greater than that of Cu-N. This may be due to the in-situ synthesis of HKUST-1 while the -COO- group in BTC is involved in the coordination of $Cu^{2+}$, resulting in a greater

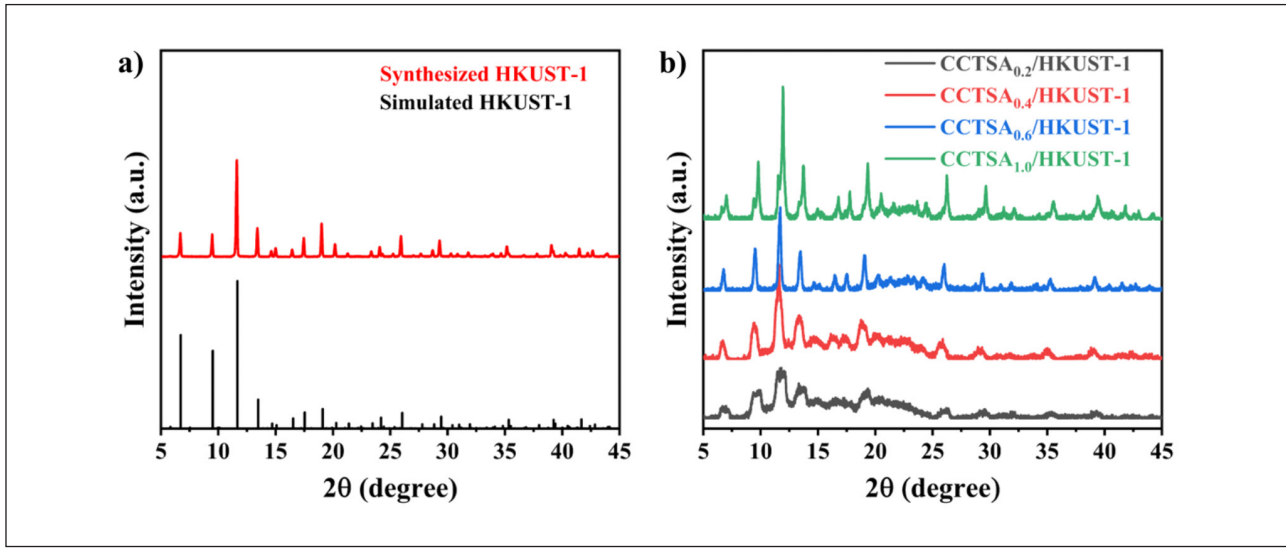


*6. X-ray diffraction (XRD) patterns: (a) comparison of synthetic and simulated HKUST-1, and (b) comparison of CCTSA/HKUST-1 composite aerogels with different CTS contents.*

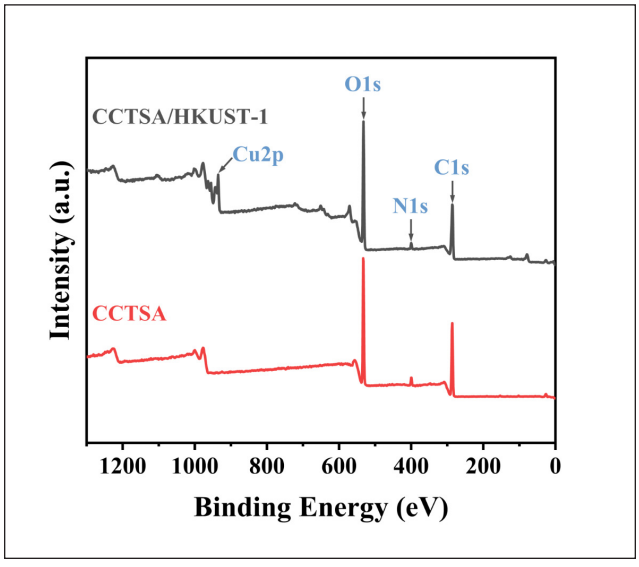


*7. X-ray photoelectron spectroscopy (XPS) survey spectra of CCTSA and CCTSA/HKUST-1.*

relative intensity of Cu-O. These XPS results indicate that HKUST-1 crystals were successfully grown in-situ on CCTSA, and that CCTSA is a suitable carrier for HKUST-1 [44,45].

**Figure 9** shows the TG and differential thermogravimetric (DTG) curves of the CCTSA/HKUST-1 composite aerogel, as well as the raw material. It can be seen that the residual contents of CCTSA are 29.74% higher than the residual content of CA at 22%, indicating that the addition of CTS is beneficial to improve the overall thermal stability of the material. The addition of HKUST-1 raised the residual contents to 31.93%, indicating that the addition of HKUST-1 further improved the thermal stability of the composite aerogel. In Fig. 9b, we can see that the decomposition temperatures of both CA and CCTSA were essentially the same at around 330°C, which may be attributed to the similar structure of cellulose and chitosan [46]. The CCTSA/HKUST-1 composite aerogel loaded with HKUST-1 showed two decomposition temperature points, and both were slightly lower than the decomposition temperatures of the corresponding CCTSA and HKUST-1, which is probably due to the formation of HKUST-1 in a strong acidic high temperature environment that caused damage to the structure of the composite aerogel, resulting in a lower decomposition temperature [47]. The mass loading rate of HKUST-1 reached 37.06% using Eq. 1, indicating that most of the HKUST-1 was loaded on CCTSA aerogel, which is an excellent carrier for HKUST-1 [4].

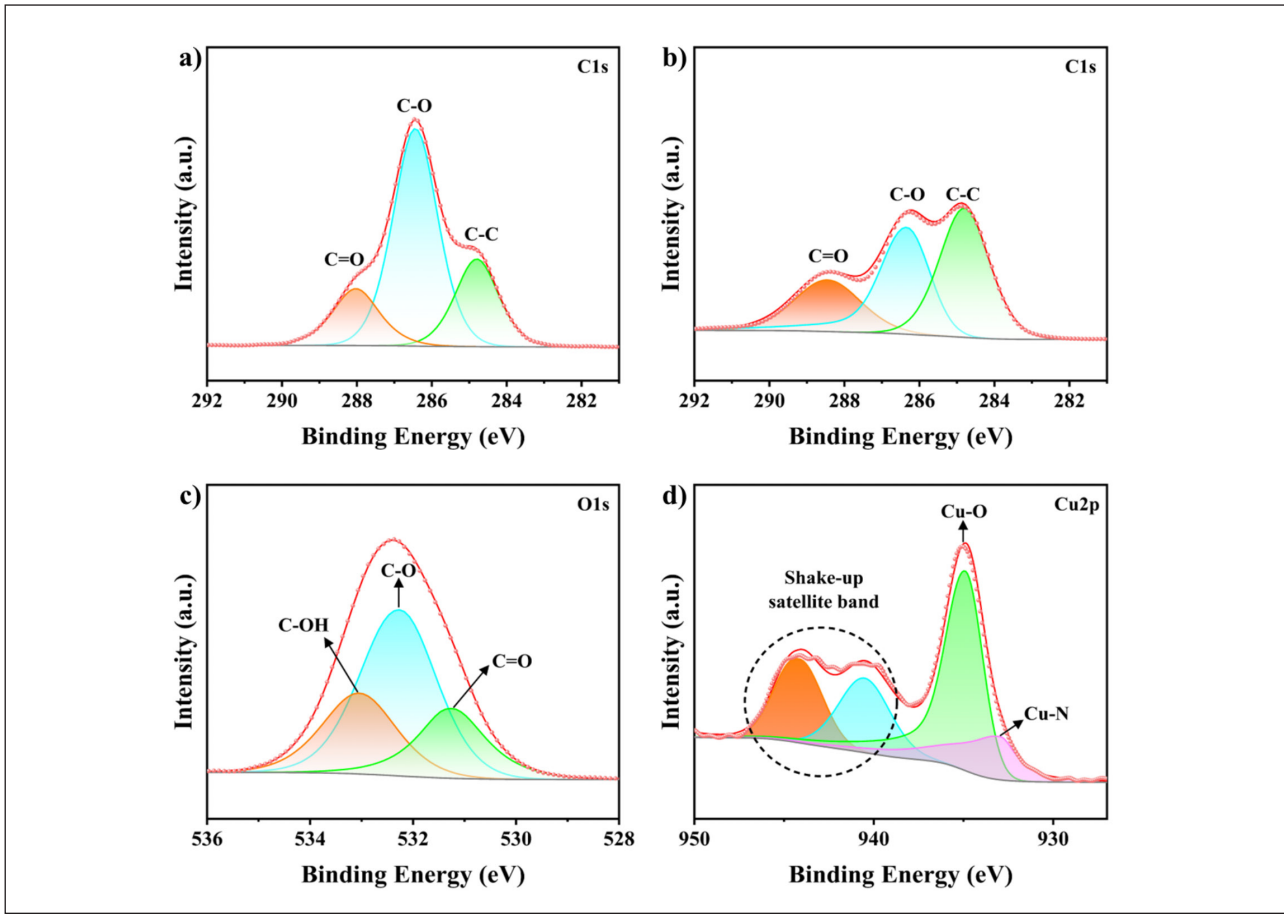


*8. The XPS patterns of composite aerogels: (a), (b) C1s survey of CCTSA and CCTSA/HKUST-1, respectively; (c) O1s survey of CCTSA/HKUST-1; and (d) Cu2p survey of CCTSA/HKUST-1.*

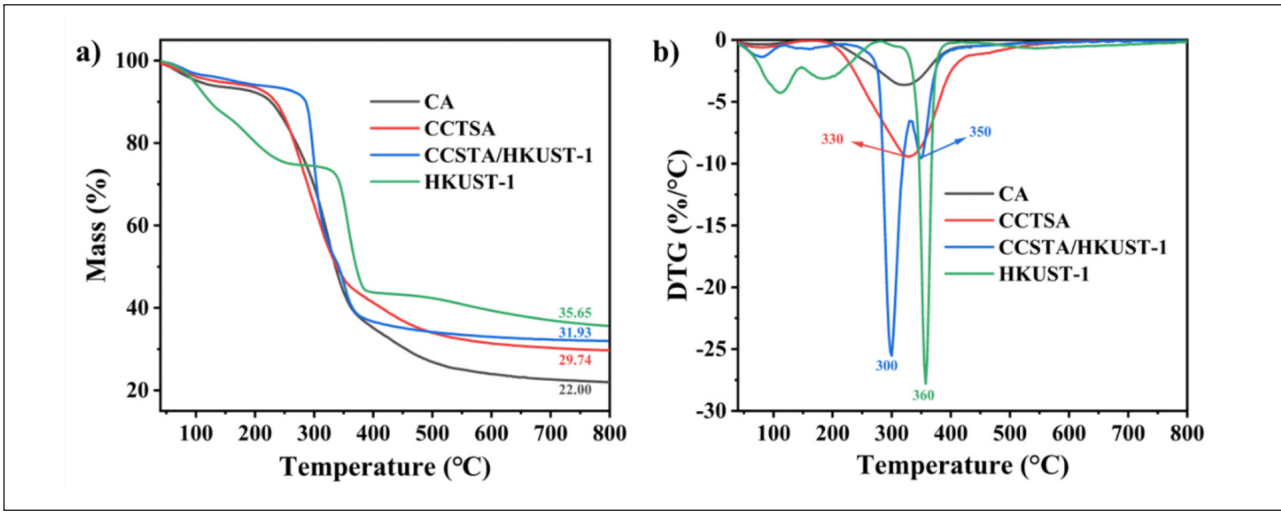


*9. (a) Thermogravimetric (TG) and (b) differential thermogravimetric (DTG) curves of composite aerogels and original HKUST-1.*

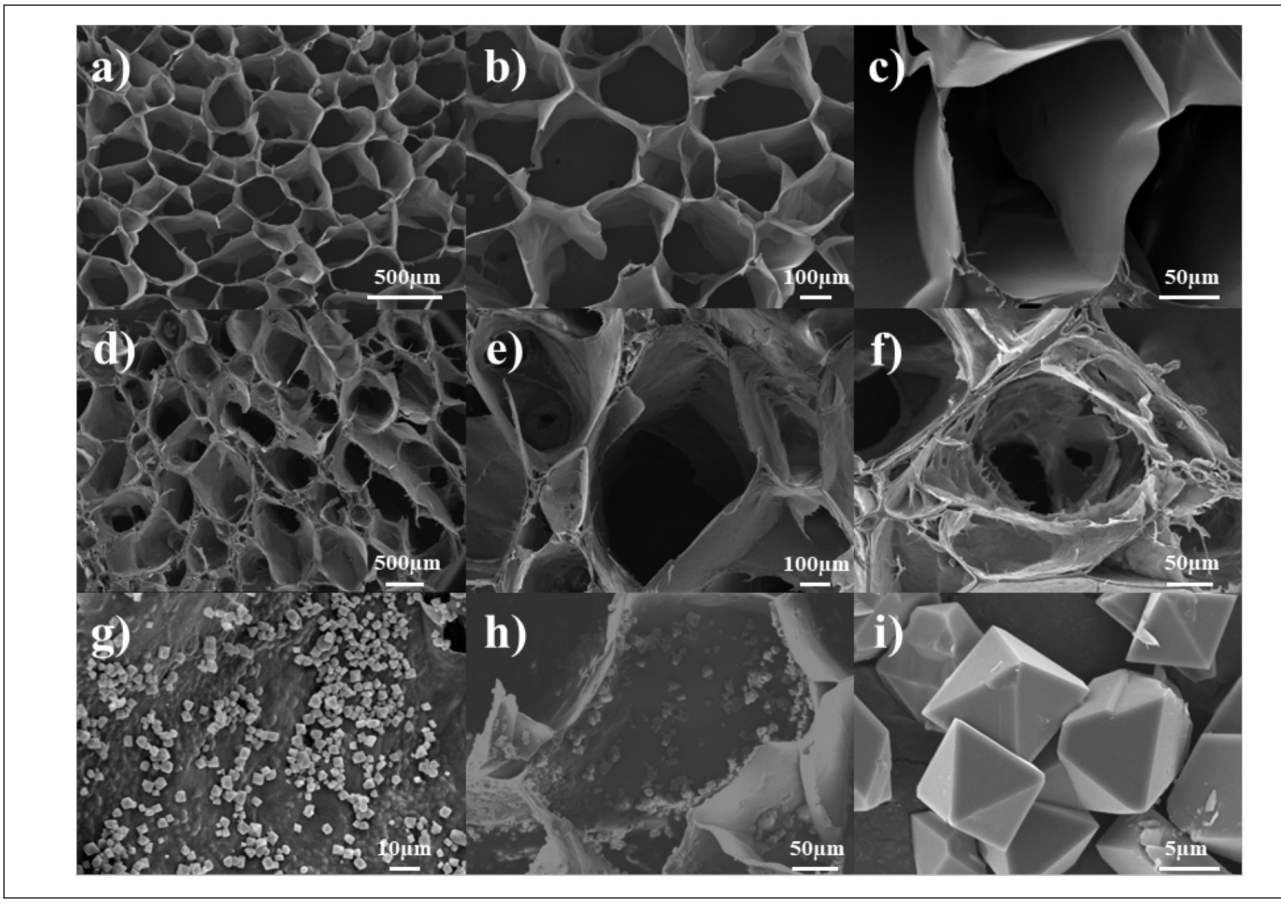


*10. Scanning electron microscopy (SEM) images: (a), (b), (c) CA; (d), (e), (f) CCTSA; (g),(h) CCTSA/HKUST-1; and (i) HKUST-1.*

The scanning electron microscopy (SEM) images of CA, CCTSA, CCTSA/HKUST-1, and HKUST-1 are shown in **Fig. 10**. From Fig. 10a–10c, CA shows the three-dimensional (3D) macroporous layered structure due to the sublimation of ice crystals during the freeze-drying process, as well as the smooth pore walls [48,49]. After the addition of CTS, the pores of the aerogel became irregular, and some folds were formed on the surface, which would be more conducive to the subsequent anchoring of HKUST-1 [4,50]. As shown in Fig. 10g–10h, after in-situ synthesis of HKUST-1, the surface of the CCTSA/HKUST-1 composite aerogel grew with octahedral HKUST-1 crystal particles as shown in Fig. 10i, and the morphology of the HKUST-1 particles was basically consistent with that reported in the literature [26].

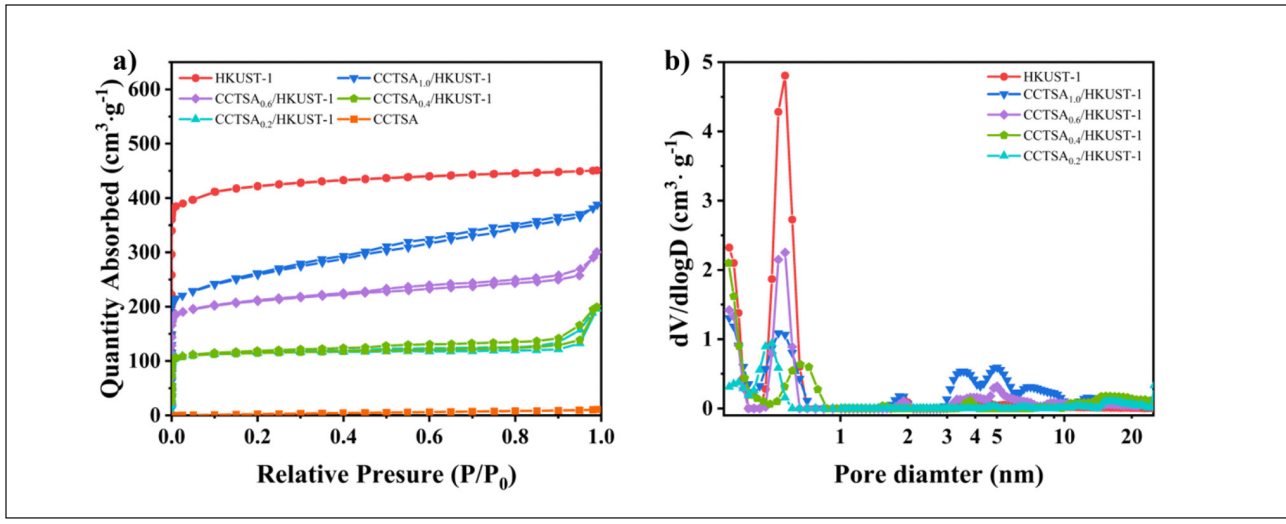


*11. (a) Nitrogen ($N_2$) adsorption and desorption isotherms, and (b) pore size distribution of CCTSA/HKUST-1 composite aerogel and HKUST-1.*

The SEM characterization illustrates the successful synthesis of CCTSA/HKUST-1.

**Figure 11a** shows the adsorption and desorption curves, and Fig. 11b shows the pore size distribution curves for CCTSA, HKUST-1, and composite aerogels with different CTS contents, while **Table I** shows the basic data for them. The basic property of an adsorbent with a high adsorption capacity is its high specific surface area [51]. The BET specific surface areas of CCTSA, $CCTSA_{0.2}$/HKUST-1, $CCTSA_{0.4}$/HKUST-1, $CCTSA_{0.6}$/HKUST-1, $CCTSA_{1.0}$/HKUST-1, and HKUST-1 are 14.489, 461.820, 463.592, 808.575, 945.123, and 1662.521 $m^2 \cdot g^{-1}$, respectively. The specific surface area of HKUST-1 is the highest, with an average pore diameter of 1.678 nm, and consists mainly of micropore/mesopore structures, while the specific surface area of CCTSA is only 14.489 $m^2 \cdot g^{-1}$, with an average pore diameter of 45.911 nm, and consists mainly of macroporous structures, so its test results show a very low BET specific surface area [38]. Compared with CCTSA, CCTSA/HKUST-1 shows a higher specific surface area. Moreover, the BET specific surface area of the composite aerogel gradually increased with the increase of CTS content, indicating that HKUST-1 had been successfully synthesized via in-situ synthesis and plays a dominant role in the contribution of the specific surface area of the composite aerogel. With higher CTS content, the loading of HKUST-1 is higher, which is because CTS is rich in N atoms that can better complex with $Cu^{2+}$ and thus promote the anchoring and in-situ synthesis of HKUST-1 on CCTSA [42,43]. In conclusion, HKUST-1 confers a high specific surface area to the composite aerogel and CTS facilitates the in-situ synthesis of HKUST-1.

### *Adsorption capacity of CCTSA/HKUST-1 for MB solution*

In **Fig. 12a**, the adsorption capacities of different adsorbents were tested for 12 h of continuous adsorption of MB solution with a concentration of 250 $mg \cdot L^{-1}$ at pH 8.0. It can be seen that the adsorption capacity of CA for MB solution was only 104.71 $mg \cdot g^{-1}$, and the adsorption capacity of CCTSA aerogel for MB solution increased to 164.87 $mg \cdot g^{-1}$ after the addition of CTS, which may be due to the addition of CTS with amino groups in the molecular structure, thus introducing more lone electron pairs and improving

| Materials | Specific Surface Area, $m^2 \cdot g^{-1}$ | Total Pore Volume, $cm^3 \cdot g^{-1}$ | Pore Diameter, nm |
|---|---|---|---|
| HKUST-1 | 1662.521 | 0.698 | 1.678 |
| CCTSA1.0/HKUST-1 | 945.123 | 0.600 | 2.539 |
| CCTSA0.6/HKUST-1 | 808.575 | 0.465 | 2.300 |
| CCTSA0.4/HKUST-1 | 463.592 | 0.309 | 2.662 |
| CCTSA0.2/HKUST-1 | 461.820 | 0.304 | 2.631 |
| CCTSA | 14.489 | 0.166 | 45.911 |

*I. The nitrogen ($N_2$) adsorption-desorption data of composite aerogels HKUST-1, $CCTSA_{1.0}$/HKUST-1; $CCTSA_{0.6}$/HKUST-1; $CCTSA_{0.4}$/HKUST-1; $CCTSA_{0.2}$/HKUST-1; and CCTSA.*

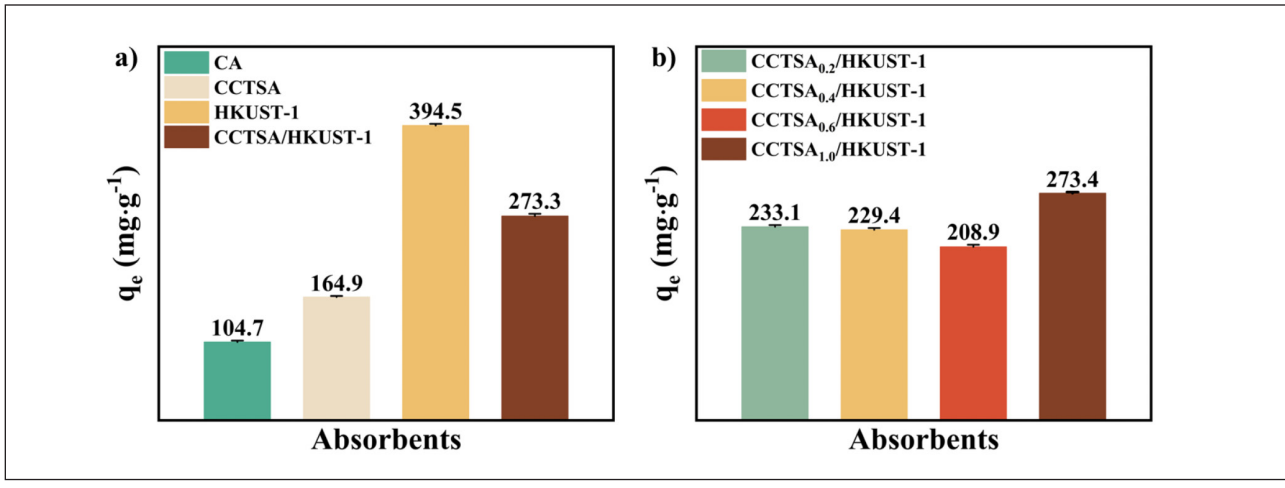


*12. Effects of (a) different absorbents and (b) the content of CTS on the methylene blue (MB) solution adsorption capacity.*

the adsorption capacity of the composite aerogel for the cationic dye MB [52,53]. The highest adsorption capacity of HKUST-1 for MB solution was 394.5 mg·g$^{-1}$, indicating that HKUST-1 is suitable for MB adsorption and is a potential MB adsorbent. The adsorption capacity of the CCTSA/HKUST-1 composite aerogel increased to 273.37 mg·g$^{-1}$ after in-situ synthesis of HKUST-1, indicating that the loading of HKUST-1 improved the adsorption capacity of the composite aerogel for MB.

In Fig. 12b, the adsorption capacities of CCTSA/HKUST-1 composite aerogels with different CTS contents were tested for 12 h under pH 8.0 using MB solution with a concentration of 250 mg·L$^{-1}$. It can be seen that the molar ratio of AGU and GSU fluctuated in the range of 0.2–0.6, but the overall adsorption capacity did not change much, and the maximum adsorption capacity was reached at $n_{AGU}$:$n_{GSU}$ = 1:1, indicating that the increase of CTS content was beneficial to improve the adsorption capacity of the composite aerogel for MB.

Reusability is an important factor for achieving cheap applications of adsorbents [54]. As shown in **Fig. 13**, the overall adsorption capacity of the regenerated composite aerogel showed a slight decreasing trend with the increase of the number of cycles. The adsorption capacity of the regenerated composite aerogel was 210.9 mg·g$^{-1}$ after one regeneration and became 199.6 mg·g$^{-1}$ after five regenerations. The recovery efficiency was maintained at 94.6%, indicating that the CCTSA/HKUST-1 composite aerogel has good reusability for MB solution.

The effect of pH of the initial solution of MB on the adsorption capacity of CCTSA/HKUST-1 composite aerogel was investigated, as shown in **Fig. 14a**. Under acidic conditions, the adsorption capacity of the CCTSA/HKUST-1 composite aerogel on MB solution gradually increased with the increase of pH. The adsorption capacity was low at pH 2–4. The adsorption capacity reached the highest at pH 8, and it began to decrease by continuing to increase the pH of the initial solution. As shown in Fig. 14b, the pH value

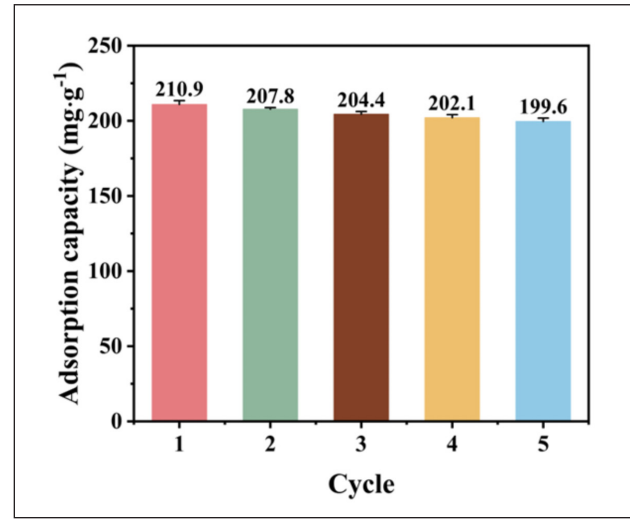


*13. Reusability of the CCTSA/HKUST-1 for MB adsorption.*

corresponding to the zero charge point ($pH_{pzc}$) of CCTSA/HKUST-1 composite aerogel was determined by the pH drift method to be 4.4 [55]. It can be seen that the ΔpH curve of CCTSA/HKUST-1 composite aerogel showed an overall decreasing trend in solution, with pH values of 2–11. When the pH value is less than the isoelectric point, the surface of the composite aerogel is positively charged and has a strong electrostatic repulsion with the cationic dye MB, which is not conducive to the adsorption of MB by the composite aerogel. At this time, the adsorption is mainly achieved by the hydrogen bonding between the O and N atoms of the composite aerogel and the N atoms of MB [4,56]. With the increase of pH, the surface of the composite aerogel is negatively charged, and the electrostatic repulsion between the composite aerogel and the cationic dye MB is gradually weakened, and the adsorption is produced by the electrostatic gravitational effect, thus improving the adsorption capacity of the composite aerogel on MB. However, at higher pH values, the generated sodium chloride (NaCl would negatively affect the adsorption capacity of the

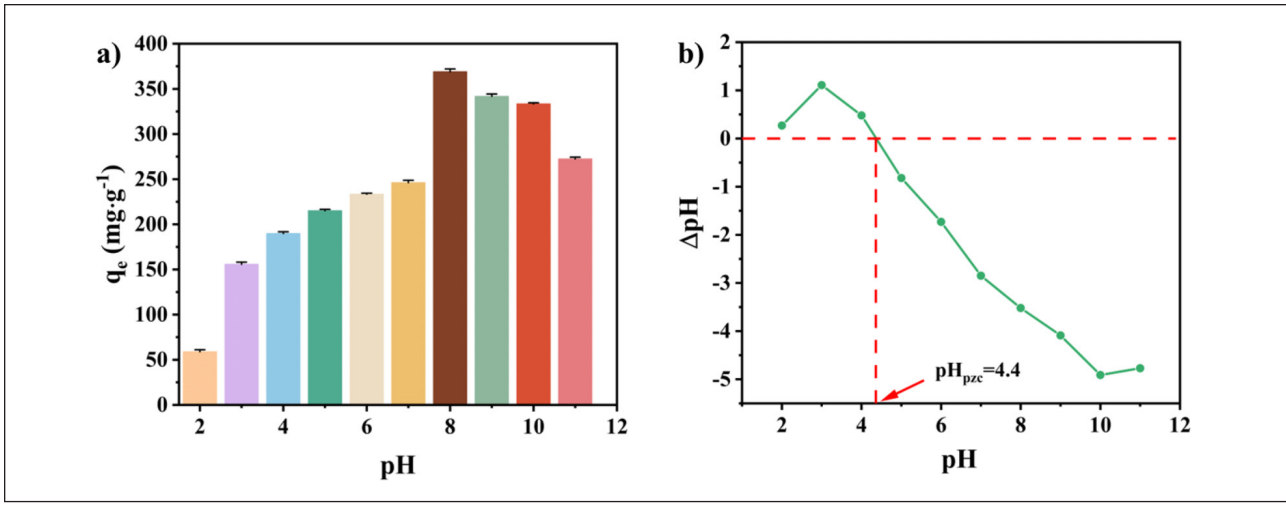


*14. (a) Effects of different initial pH value on the MB solution adsorption capacity, and (b) the zero charge point ($pH_{pzc}$) of CCTSA/HKUST-1 composite aerogel.*

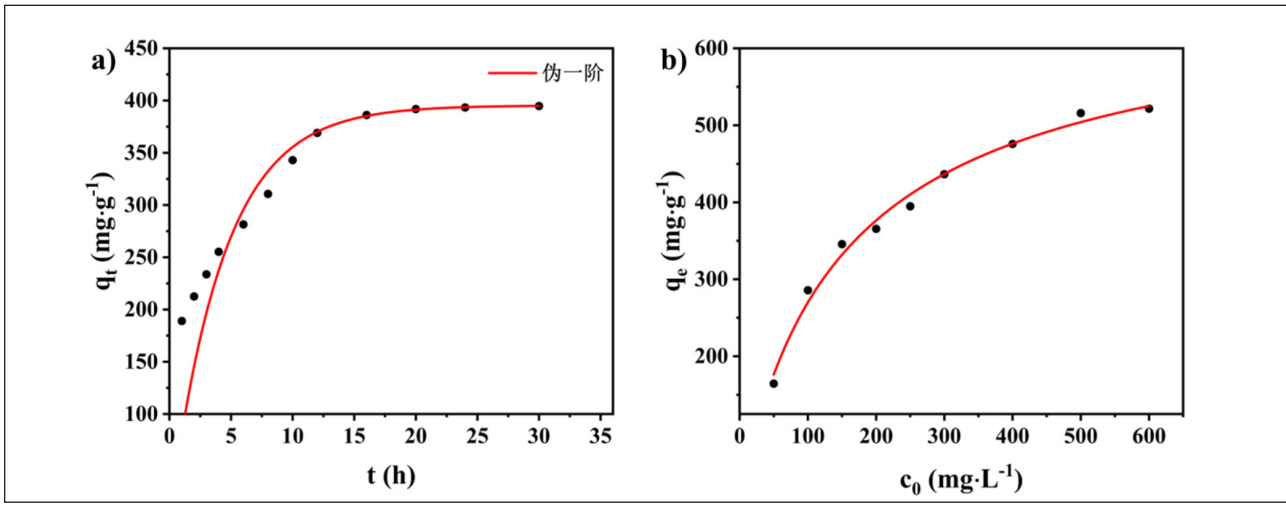


*15. Effects of (a) adsorption time and (b) initial concentration on the MB adsorption capacity.*

composite aerogel [4]. Therefore, a pH value of 8.0 was chosen for the next experiments.

As shown in **Fig. 15**, the adsorption capacity of CCTSA/HKUST-1 composite aerogel was tested at different adsorption times using MB solution at a concentration of 250 mg·L$^{-1}$ at pH 8.0. The adsorption capacity increased from 189.0 mg·g$^{-1}$ at 1 h to 386.2 mg·g$^{-1}$ at 16 h. The adsorption capacity remained the same at 30 h, indicating that the adsorption of MB by the CCTSA/HKUST-1 composite aerogel had reached saturation at this time. The adsorption data were fitted by the pseudo-first-order and pseudo-second-order adsorption kinetic models of Eq. 3 and Eq. 4, and the results and data are shown in **Fig. 16a–6b** and **Table II**. It can be seen that the fitted coefficient of determinaton $R^2 > 0.99$ for the pseudo-second-order adsorption kinetic model indicates that this model is highly consistent with the adsorption process and that the adsorption process is mainly chemisorption [57]. However, the fitted $R^2$ of the pseudo-first-order adsorption kinetic model reaches 0.980, which indicates that the adsorption process is also physisorption [4,58]. In summary, the whole adsorption process is the result of the dominant chemisorption and the synergistic effect of physical adsorption.

As indicated in Fig. 15b, the adsorption capacity of CCTSA/HKUST-1 composite aerogel was tested at different initial concentrations for 24 h continuously using MB solution with concentrations ranging from 50 to 600 mg·L$^{-1}$ at pH 8.0. It was observed that the increase rate of the adsorption capacity of CCTSA/HKUST-1 composite aerogel on MB decreased gradually with the increase of the initial concentration of MB solution. The adsorption capacity of the composite aerogel increased from 164.5 mg·g$^{-1}$ to 521.6 mg·g$^{-1}$ when the initial concentration was increased from 50 mg·L$^{-1}$ to 600 mg·L$^{-1}$, and the adsorption capacity of the composite aerogel on MB solution remained basically unchanged when the initial concentration was in the range of 500–600 mg·L$^{-1}$, indicating that the adsorption of the composite aerogel on MB solution had reached satura-

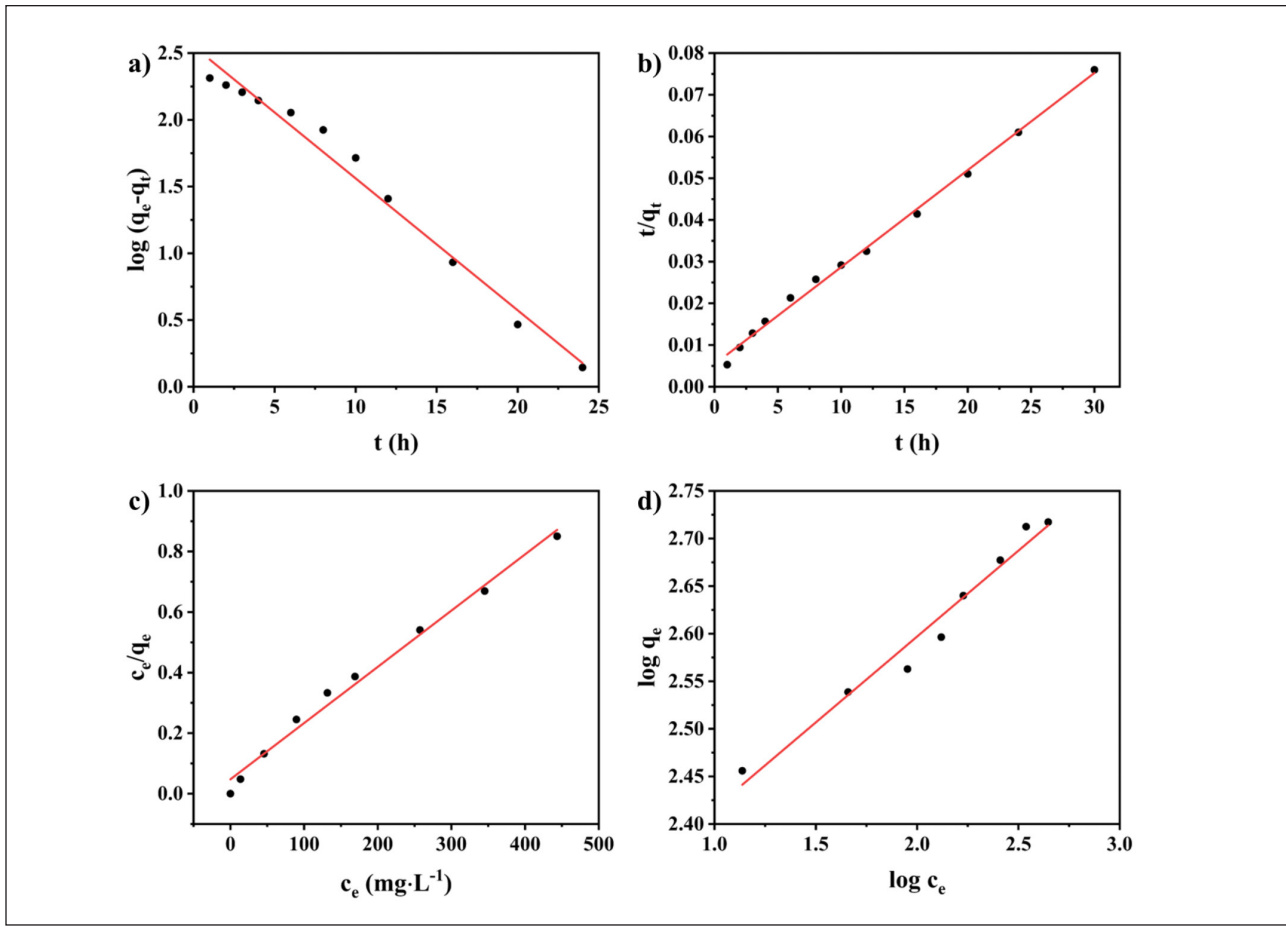


*16. Fitting of CCTSA/HKUST-1 composite aerogels on MB solution adsorption capacity by: (a) pseudo-first-order adsorption kinetics; (b) pseudo-second-order adsorption kinetics; (c) Langmuir adsorption isotherm; and (d) Freundlich adsorption isotherm models.*

tion. The data were fitted by the Langmuir and Freundlich adsorption models of Eq. 5 and Eq. 6, and the results of the fitted curves and correlation parameters are shown in Fig. 16c–16d and **Table III**. According to the results of the fitted coefficient of determination $R^2$, the Langmuir adsorption model is more suitable for describing the adsorption behavior of the composite aerogel on MB solution, which is mainly dominated by the chemisorption of the monolayer. Also, the Freundlich adsorption model exhibits a good correlation between the initial concentration of the MB solution and the adsorption capacity of the composite aerogel on the MB solution, indicating that the adsorption process also exists in the physical adsorption of multiple layers [4,67]. Therefore, the adsorption process of CCTSA/HKUST-1 composite aerogel on MB solution includes chemisorption of monolayer as well as physical adsorption of multilayer. The maximum theoretical adsorption capacity ($q_{max}$) of CCTSA/HKUST-1 composite aerogel on MB solution was calculated from the Langmuir adsorption model as 537.6 mg·g$^{-1}$. The adsorption capacities of various HKUST-1-based adsorbents, polysaccharide-based aerogels, and pure HKUST-1 crystals for MB solution in recent years are compared in **Table IV**. The maximum theoretical adsorption capacity qmax of pure HKUST-1 crystals on MB solu-

| $q_e$, mg·g$^{-1}$ (experimental) | Pseudo-first-order Model | | | Pseudo-second-order Model | | |
|---|---|---|---|---|---|---|
| | $q_e$, mg·g$^{-1}$ (theoretical) | $k_1$, h$^{-1}$ | $R^2$ | $q_e$, mg·g$^{-1}$ (theoretical) | $k_2$, g·mg$^{-1}$·h$^{-1}$ | $R^2$ |
| 394.8 | 355.1 | 0.228 | 0.980 | 429.2 | 1.005×10-3 | 0.996 |

$q_e$: saturation adsorption capacity; $k_1$ and $k_2$: pseudo-first-order and pseudo-second-order rate constants, respectively; $R^2$: coefficient of determination.

*II. Fitting parameters of pseudo-first-order and pseudo-second-order adsorption kinetic models.*

| $q_e$, mg·g$^{-1}$ (experimental) | Langmuir | | | Freundlich | | |
|---|---|---|---|---|---|---|
| | $q_{max}$, mg·g$^{-1}$ (theoretical) | $K_L$, L·mg$^{-1}$ | $R^2$ | $K_F$, mg·g$^{-1}$ | $n$ | $R^2$ |
| 521.6 | 537.6 | 0.039 | 0.987 | 172.2 | 5.540 | 0.965 |

$q_e$: saturation adsorption capacity; $K_L$ and $q_{max}$: Langmuir constants for the monolayer and adsorption energy related to $q_e$, respectively; $K_F$ (mg·g$^{-1}$) and $n$: Freundlich constants representing the adsorption capacity and adsorption intensity, respectively; $R^2$: coefficient of determination.

***III. Fitting parameters of adsorption isotherm model.***

| Absorbent | $q_{max}$, mg·g$^{-1}$ | Reference |
|---|---|---|
| ($Fe_3O_4$, $TiO_2$)/HKUST-1 | 767 | 59 |
| HP-HKUST-1 | 241 | 60 |
| HKUST-1/GO | 183.49 | 61 |
| F-CNTs@MOF@Gel | 106.5 | 56 |
| HKUST-1@PVA-co-PE/PVA | 481.5 | 62 |
| HKUST-1 | 458.4 | 63 |
| HKUST-1/CCSA | 526.3 | 4 |
| CS/EDTA/CBC | 590.72 | 64 |
| Cellulose/AC | 159 | 65 |
| CSCC | 95.31 | 66 |
| CCTSA/HKUST-1 | 537.6 | Current work |

$q_{max}$: Langmuir constant for adsorption energy related to saturation adsorption capacity $q_e$.

***IV. Comparison of the adsorption capacity of various HKUST-1-based adsorbents and polysaccharide-based aerogels for methylene blue (MB) solution.***

tion was 458.4 mg·g$^{-1}$ [63], while the $q_{max}$ of cellulose/AC aerogel and CSCC aerogel were only 159 mg·g$^{-1}$ and 95.31 mg·g$^{-1}$ [65,66], which fully demonstrated the excellent adsorption capacity of the CCTSA/HKUST-1 composite aerogel prepared in this work on MB solution.

As shown in **Fig. 17**, the adsorption capacity of CCTSA/HKUST-1 composite aerogel was tested at different adsorption temperatures using MB solution at a concentration of 250 mg·L$^{-1}$ at pH 8.0. The adsorption capacity decreases with increasing adsorption temperature, but the change is not significant, as can be seen from Fig. 17a. The adsorption data were fitted by Eq. 7 and Eq. 8, and the fitted curves and related parameters are shown in Fig. 17b and **Table V**. It can be seen that the change of Gibbs free energy $\Delta G^o$ is always negative, indicating that the adsorption process of MB solution by CCTSA/HKUST-1 composite aerogel is spontaneous. The entropy change $\Delta S^o$ presents a positive value, indicating that the temperature rise increases the disorder of the system. The enthalpy change $\Delta H^o$ presents negative values, indicating that the whole adsorption process is exothermic, so the increase in temperature prevents the adsorption reaction and makes the adsorption capacity decrease with the increase in adsorption temperature, which is consistent with the results shown in Fig. 17a [54,67].

## CONCLUSION

As this research has demonstrated, CCTSA/HKUST-1 composite aerogels were prepared by a simple and green method. The successful in-situ synthesis of HKUST-1 has increased the BET specific surface area of CCTSA/HKUST-1 composite aerogel to 945.123 m$^2$·g$^{-1}$, and it has excellent adsorption capacity on MB solution and is capable of cyclic adsorption. The adsorption mechanism of CCTSA/HKUST-1 composite aerogel on MB solution was analyzed by the synergistic effect of monolayer chemisorption and multilayer physical adsorption. This study will provide theoretical and technical support for the design and preparation of polysaccharide-based aerogel adsorption materials with high adsorption capacity, and broaden the application of MOFs materials in the field of water treatment. **TJ**

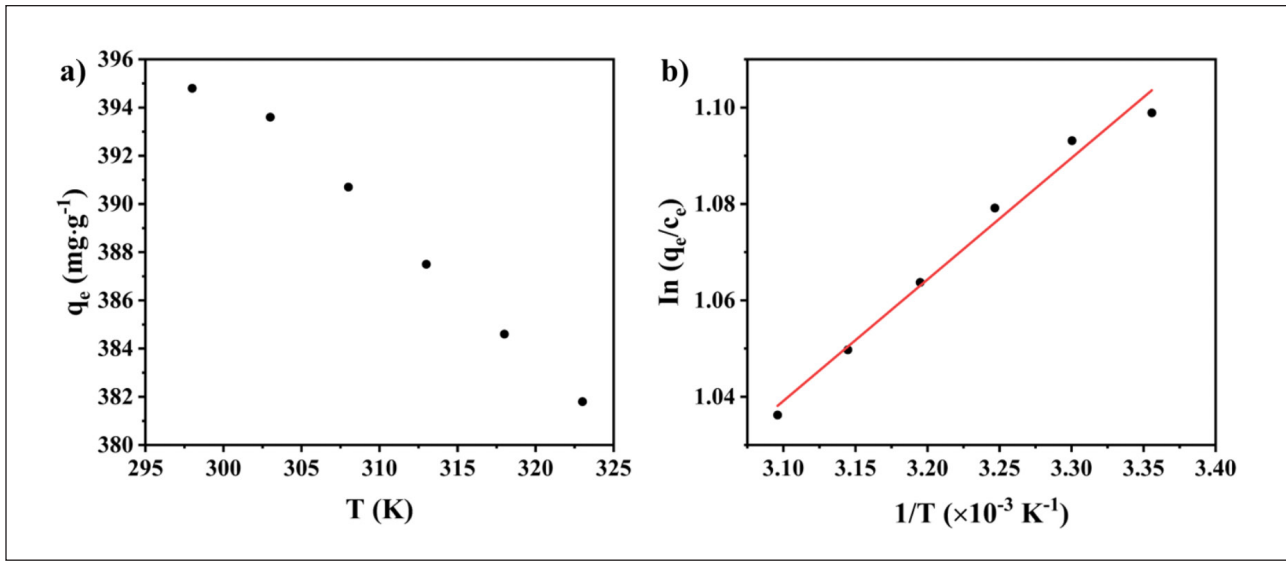


***17. (a) Effects of different temperature on the MB solution adsorption capacity, and (b) adsorption thermodynamic fitting curve.***

| *ΔH°*, kJ·mol$^{-1}$ | *ΔS°*, J·K-1·mol$^{-1}$ | *ΔG°*, kJ·mol$^{-1}$ | | | | | |
|---|---|---|---|---|---|---|---|
| -2.09 | 2.15 | 298K | 303K | 308K | 313K | 318K | 323K |
| | | -2.731 | -2.741 | -2.752 | -2.763 | -2.774 | -2.784 |
| ΔH° : enthalpy change during adsorption; ΔS°: entropy change during adsorption; ΔG°: Gibbs free energy change. | | | | | | | |

***V. Adsorption thermodynamic parameters.***


## ACKNOWLEDGEMENTS

This work was supported by the National Natural Science Foundation of China (no. 31700516).


## LITERATURE CITED


1. Najafi, M., Abednatanzi, S., Gohari Derakhshandeh, P., et al., *Coord. Chem. Rev.* 454: 214332(2022). https://doi.org/10.1016/j.ccr.2021.214332.
2. Sriram, G., Bendre, A., Mariappan, E., et al., *Sustainable Mater. Technol.* 31: e00378(2022). https://doi.org/10.1016/j.susmat.2021.e00378.
3. Jeong, C., Ansari, M.Z., Hakeem Anwer, A., et al., *Sep. Purif. Technol.* 305: 122416(2023). https://doi.org/10.1016/j.seppur.2022.122416.
4. Liu, Q., Yu, H., Zeng, F., et al., *Carbohydr. Polym.* 255: 117402(2021). https://doi.org/10.1016/j.carbpol.2020.117402.
5. Jayasuriya, D.M.N.H. and Nadarajah, K., *Water Sci. Eng.* 16(2): 154(2023). https://doi.org/10.1016/j.wse.2022.12.006.
6. Chiam, S.-L., Pung, S.-Y., and Yeoh, F.-Y., *Environ. Sci. Pollut. Res.* 27(6): 5759(2020). https://doi.org/10.1007/s11356-019-07568-8.
7. El Messaoudi, N., El Khomri, M., El Mouden, A., et al., *Biomass Conv. Biorefin.* 14: 11739(2024). https://doi.org/10.1007/s13399-022-03604-9.
8. Li, C.J., Zhang, Y.J., Chen, H., et al., *J. Cleaner Prod.* 348: 131278(2022). https://doi.org/10.1016/j.jclepro.2022.131278.
9. Blaga, A.C., Zaharia, C., and Suteu, D., *Polymers* 13(17): 2893(2021). https://doi.org/10.3390/polym13172893.
10. Xiaoliang, Q., Xianqin, T., Wenhao, P., et al., *J. Cleaner Prod.* 315: 128221(2021). https://doi.org/10.1016/j.jclepro.2021.128221.
11. Cheng, H., Gu, B., Pennefather, M.P., et al., *Mater. Des.* 130: 452(2017). https://doi.org/10.1016/j.matdes.2017.05.082.
12. Duong, H.M., Lim, Z.K., Nguyen, T.X., et al., *Colloids Surf., A* 537: 502(2018). https://doi.org/10.1016/j.colsurfa.2017.10.067.
13. Wang, J. and Liu, S., *Sep. Purif. Technol.* 221: 303(2019). https://doi.org/10.1016/j.seppur.2019.03.097.
14. Dongxue, H., Hongjie, Z., Lili, G., et al., *Colloids Surf., A* 628: 127355(2021). https://doi.org/10.1016/j.colsurfa.2021.127355.
15. Sessarego, S., Rodrigues, S.C.G., Xiao, Y., et al., *Carbohydr. Polym.* 211: 249(2019). https://doi.org/10.1016/j.carbpol.2019.02.003.
16. Abdul Khalil, H.P.S, Saurabh, C.K., Adnan, A.S., et al., *Carbohydr. Polym.* 150: 216(2016). https://doi.org/10.1016/j.carbpol.2016.05.028.
17. Ahmadijokani, F., Molavi, H., Bahi, A., et al., *Adv. Funct. Mater.* 32(51): 2207723(2022). https://doi.org/10.1002/adfm.202207723.
18. Maru, K., Kalla, S., and Jangir, R., *New J. Chem.* 46(7): 3054(2022). https://doi.org/10.1039/d1nj05015j.
19. Ying, T., Su, J., Jiang, Y., et al., *J. Mater. Chem. A* 10(2): 829(2022). https://doi.org/10.1039/d1ta04982h.
20. Masoomi, M.Y., Morsali, A., Dhakshinamoorthy, A., et al., *Angew. Chem., Int. Ed.* 58(43): 15188(2019). https://doi.org/10.1002/anie.201902229.

21. Shi, Y., Yang, A.-F., Cao, C.-S., et al., *Angew. Chem., Int. Ed.* 390: 50(2019). https://doi.org/10.1016/j.ccr.2019.03.012.
22. Tchinsa, A., Hossain, M.F., Wang, T., et al., *Chemosphere* 284: 131393(2021). https://doi.org/10.1016/j.chemosphere.2021.131393.
23. Bingbing, Y., Yang, L., Zhiyin, L., et al., *Chem. Eng. J.* 455: 140840(2023). https://doi.org/10.1016/j.cej.2022.140840.
24. Hammi, N., Chen, S., Primo, A., et al., *Green Chem.* 24(11): 4533(2022). https://doi.org/10.1039/d2gc00097k.
25. Liu, A., Liu, J., He, S., et al., *Int. J. Biol. Macromol.* 255: 40(2023). https://doi.org/10.1016/j.ijbiomac.2022.11.321.
26. Goyal, P., Paruthi, A., Menon, D., et al., *Chem. Eng. J.* 430: 133088(2022). https://doi.org/10.1016/j.cej.2021.133088.
27. Huang, H., Ge, H., Song, J., et al., *ACS Sustainable Chem. Eng.* 7(1): 618(2019). https://doi.org/10.1021/acssuschemeng.8b04177.
28. Liang, X., Duan, J., Xu, Q., et al., *Chem. Eng. J.* 317: 766(2017). https://doi.org/10.1016/j.cej.2017.02.089.
29. Sun, J., Shang, M., Zhang, M., et al., *Carbohydr. Polym.* 293: 119720(2022). https://doi.org/10.1016/j.carbpol.2022.119720.
30. Li, L., Liu, X.L., Geng, H.Y., et al., *J. Mater. Chem. A* 1(35): 10292(2013). https://doi.org/10.1039/c3ta11478c.
31. Wang, S., Lu, A., and Zhang, L., *Prog. Polym. Sci.* 53: 169(2016). https://doi.org/10.1016/j.progpolymsci.2015.07.003.
32. Lue, A. and Zhang, L., "Advances in aqueous cellulose solvents," in *Cellulose Solvents: For Analysis, Shaping and Chemical Modification, ACS Symp. Ser.*, American Chemical Society, Washington, D.C., 2010, Chap. 3, pp. 67-89. https://doi.org/10.1021/bk-2010-1033.ch003
33. Yang, J., Medronho, B., Lindman, B., et al., *Polymers* 12(2): 373(2020). https://doi.org/10.3390/polym12020373.
34. Zhao, R., Ma, T., Zhao, S., et al., *Chem. Eng. J.* 382: 122893(2020). https://doi.org/10.1016/j.cej.2019.122893.
35. Chung, C., Lee, M., and Choe, E.K., *Carbohydr. Polym.* 58(4): 417(2004).https://doi.org/10.1016/j.carbpol.2004.08.005.
36. Cesco, C.T., Valente, A.J.M., and Paulino, A.T., *Pharmaceutics* 13(6): 842(2021).https://doi.org/10.3390/pharmaceutics13060842.
37. Zhang, S., Feng, J., Feng, J., et al., *Appl. Surf. Sci.* 396: 1220(2017). https://doi.org/10.1016/j.apsusc.2016.11.116.
38. Geng, H., *Int. J. Biol. Macromol.* 118: 921(2018). https://doi.org/10.1016/j.ijbiomac.2018.06.167.
39. Karkhani, R. and Javanbakht, V., *Int. J. Biol. Macromol.* 213: 699(2022). https://doi.org/10.1016/j.ijbiomac.2022.05.120.
40. Wang, C., Qian, X., and An, X., *Cellulose* 22(6): 3789(2015). https://doi.org/10.1007/s10570-015-0754-4.
41. Xiang, S., Zhou, W., Gallegos, J.M., et al., *J. Am. Chem. Soc.* 131(34): 12415(2009). https://doi.org/10.1021/ja904782h.
42. Wang, G., Wang, J., Chen, Z., et al., *Int. J. Biol. Macromol.* 206(2022): 232(2022). https://doi.org/10.1016/j.ijbiomac.2022.02.010.
43. Wisser, D., Wisser, F.M., Raschke, S., et al., *Angew. Chem., Int. Ed.* 54(43): 12588(2015). https://doi.org/10.1002/anie.201504572.
44. Huang, G., Li, Y., Qin, Z., et al., *Carbohydr. Polym.* 233: 115848(2020). https://doi.org/10.1016/j.carbpol.2020.115848.
45. Han, S., Ciufo, R.A., Meyerson, M.L., et al., *J. Mater. Chem. A* 7: 19396(2019). https://doi.org/10.1039/c9ta05179a.
46. He, M., Chen, H., Zhang, X., et al., *Cellulose* 25: 1987(2018). https://doi.org/10.1007/s10570-018-1683-9.
47. Cui, X., Sun, X., Liu, L., et al., *Chem. Eng. J.* 369: 898(2019). https://doi.org/10.1016/j.cej.2019.03.129.
48. Ambaye, T.G., Vaccari, M., Prasad, S., et al., *J. Environ. Manage.* 301: 113850(2022).https://doi.org/10.1016/j.jenvman.2021.113850.
49. Geng, H., Qin, M., and Li, J., *Int. J. Biol. Macromol.* 217: 417(2022). https://doi.org/10.1016/j.ijbiomac.2022.07.076.
50. Andrieux, S., Medina, L., Herbst, M., et al., *Composites, Part A* 125: 105516(2019). https://doi.org/10.1016/j.compositesa.2019.105516.
51. Pan, R., Tang, Y., Guo, Y., et al., *Microporous Mesoporous Mater.* 323: 111197(2021). https://doi.org/10.1016/j.micromeso.2021.111197.
52. Fan, X., Wang, X., Cai, Y., et al., *J. Hazard. Mater.* 423: 127191(2022). https://doi.org/10.1016/j.jhazmat.2021.127191 .
53. Salama, A. and Abou-Zeid, R.E., *Int. J. Biol. Macromol.* 188: 404(2021). https://doi.org/10.1016/j.ijbiomac.2021.08.021.
54. Zhu, R., Xia, J., Zhang, H., et al., *J. Environ. Chem. Eng.* 9(6): 106538(2021). https://doi.org/10.1016/j.jece.2021.106538.
55. Liu, J., Dong, Y., Zhang, L., et al., *J. Cleaner Prod.* 322: 129059(2021). https://doi.org/10.1016/j.jclepro.2021.129059.
56. Zhang, Y., Li, Y., Wang, M., et al., *Nanomaterials* 12(15): 2533(2022). https://doi.org/10.3390/nano12152533.
57. Fei, Y., Xueting, B., Mingxing, L., et al., *Sep. Purif. Technol.* 288: 120647(2022). https://doi.org/10.1016/j.seppur.2022.120647.
58. Zhao, L., Azhar, M.R., Li, X., et al., *J. Colloid Interface Sci.* 542: 421(2019). https://doi.org/10.1016/j.jcis.2019.01.117.
59. Kubo, M., Moriyama, R., and Shimada, M., *Microporous Mesoporous Mater.* 280: 227(2019). https://doi.org/10.1016/j.micromeso.2019.02.010.
60. Bai, K., Fan, S., Chen, Y., et al., *J. Membr. Sci.* 650: 120424(2022). https://doi.org/10.1016/j.memsci.2022.120424.
61. Li, L., Liu, X.L., Geng, H.Y., et al., *J. Mater. Chem. A* 1(35): 10292(2013). https://doi.org/10.1039/c3ta11478c.
62. Zhu, Q., Li, Y., Wang, W., et al., *Compos. Commun.* 10: 36(2018). https://doi.org/10.1016/j.coco.2018.05.005.
63. Lin, S., Song, Z., Che, G., et al., *Microporous Mesoporous Mater.* 193: 27(2014). https://doi.org/10.1016/j.micromeso.2014.03.004.
64. Fan, X., Wang, X., Cai, Y., et al., *J. Hazard. Mater.* 423: 127191(2022). https://doi.org/10.1016/j.jhazmat.2021.127191.
65. Bai, Q., Xiong, Q., Li, C., et al., *Cellulose* 24: 4275(2017). https://doi.org/10.1007/s10570-017-1410-y.
66. Marrakchi, F., Hameed, B.H., and Hummadi, E.H., *Int. J. Biol. Macromol.* 163: 1079(2020). https://doi.org/10.1016/j.ijbiomac.2020.07.032.
67. Ma, X., Wang, L., Wang, H., et al., *J. Hazard. Mater.* 424: 126918(2022). https://doi.org/10.1016/j.jhazmat.2021.126918.

## ABOUT THIS PAPER

**Cite this article as**:
Wang, T., Wang, L., Liu, S., et al., *TAPPI J.* 23(528): 10(2024). https://doi.org/10.32964/TJ23.10.528

**DOI:** https://doi.org/10.32964/TJ23.10.528

**ISSN:** 0734-1415

**Publisher:** TAPPI Press





*About this journal*


## ABOUT THE AUTHORS

This study will provide theoretical and technical support for the design and preparation of stable polysaccharide aerogel adsorbent materials with high adsorption capacity. The most difficult part of the study was preparing the CCTSA/HKUST-1 composite aerogel, but through trial and error, we succeeded. Our most interesting findings were related to the characterization of CCTSA/HKUST-1, and our next steps will focus on further investigation of the nature, role, and extended uses of this composite aerogel.

***T. Wang***

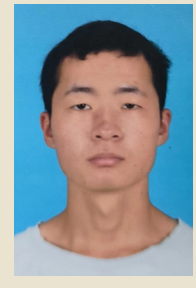

***L. Wang***

***S. Liu***

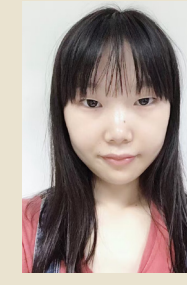

***Chen***

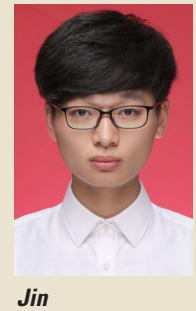

***Jin***

***H. Liu***

***Liao***


*T. Wang and L. Wang are undergraduate students; S. Liu, Chen, and Jin are graduate students; and H. Liu and Liao are associate professors at Tianjin University of Science and Technology in Tianjin, P.R. China. Email H. Liu at liuhaitang@tust.edu.cn.*


(Note: In this manuscript, T. Wang and L. Wang provided writing and reviewing; S. Liu provided editing; Chen provided conceptualization, methodology, software support, investigation, drawing application, data curation, and writing of original draft; Jin provided software support, writing, and reviewing; H. Liu provided supervision, funding acquisition, conceptualization, writing, reviewing, and editing; and Liao provided supervision.)